Observational constraints on Myrzakulov gravity

Fotios K. Anagnostopoulos,[1,*] Spyros Basilakos,[2,3,†] and Emmanuel N. Saridakis[3,4,5,‡]

[1]*Department of Physics, National & Kapodistrian University of Athens, Zografou Campus GR 157 73 Athens, Greece*

[2]*Academy of Athens, Research Center for Astronomy and Applied Mathematics, Soranou Efesiou 4, 11527 Athens, Greece*

[3]*National Observatory of Athens, Lofos Nymfon, 11852 Athens, Greece*

[4]*CAS Key Laboratory for Researches in Galaxies and Cosmology, Department of Astronomy, University of Science and Technology of China, Hefei, Anhui 230026, People's Republic of China*

[5]*School of Astronomy, School of Physical Sciences, University of Science and Technology of China, Hefei 230026, People's Republic of China*

(Received 29 December 2020; accepted 13 April 2021; published 10 May 2021)

We use data from Supernovae Pantheon sample, from baryonic acoustic oscillations, and from cosmic chronometers measurements of the Hubble parameter, alongside arguments from big bang nucleosynthesis, in order to extract constraints on Myrzakulov $F(R,T)$ gravity. This is a connection-based theory belonging to the Riemann-Cartan subclass, that uses a specific but nonspecial connection, which then leads to extra degrees of freedom. Our analysis shows that both considered models lead to approximately 1σ compatibility in all cases. For the involved dimensionless parameter, we find that it is constrained to an interval around zero; however, the corresponding contours are slightly shifted toward positive values. Furthermore, we use the obtained parameter chains to reconstruct the corresponding Hubble function, as well as the dark energy equation-of-state parameter, as a function of redshift. As we show, model 1 is very close to Λ-Cold Dark Matter (ΛCDM) scenario, while model 2 resembles it at low redshifts; however, at earlier times, deviations are allowed. Finally, applying the Akaike Information Criterion, Bayesian Information Criterion, and combined Deviance Information Criterion criteria, we deduce that both models present a very efficient fitting behavior and are statistically equivalent with ΛCDM cosmology, despite the fact that model 2 does not contain the latter as a limit.

DOI: 10.1103/PhysRevD.103.104013

I. INTRODUCTION

According to the concordance cosmological model, the Universe experienced two epochs of accelerated expansion, one at early and one at late times. Although the latter can be explained by the presence of a cosmological constant, the related theoretical problem, the possibility of a dynamical behavior, and especially the inability of the cosmological constant to describe the early accelerated phase led to the incorporation of some form of modification. As a first possibility, one can maintain general relativity as the underlying theory and modify the matter content of the Universe by introducing extra fields, such as the inflaton at early times [1,2] and/or the dark energy sector at late times [3,4]. As a second possibility, one modifies the gravitational sector itself, constructing a theory that possesses general relativity as a particular limit but which in general exhibits extra degrees of freedom [5,6].

There are many ways to construct gravitational modifications, each one modifying a particular feature of general relativity. Modifying the dimensionality gives rise to the braneworld theories [7]; modifying the Einstein-Hilbert Lagrangian gives rise to $F(R)$ gravity [8,9], $F(G)$ gravity [10,11], Lovelock theories [12,13], etc.; and adding a scalar field coupled with curvature in various ways gives rise to Horndeski/Galileon theories [14–16]. Additionally, starting from the equivalent, teleparallel, formulation of gravity [17,18], one can construct modifications using torsional invariants, such as in $F(T)$ gravity [19,20], in $F(T,T_G)$ gravity [21], or in scalar-torsion theories [22,23]. Moreover, one can construct the general class of metric-affine theories [24–26], which incorporates a general linear connection structure, or proceed to the introduction of nonlinear connections such as in Finsler and Finsler-like theories [27–32].

Inspired by these, one could start from such affinely connected metric theories, and in particular from their Riemann-Cartan subclass [33], and construct a theory using a specific but nonspecial connection, which would lead to

*fotis-anagnostopoulos@hotmail.com
†svasil@academyofathens.gr
‡msaridak@noa.gr

 © 2021 American Physical Society

nonzero torsion and nonzero curvature at the same time, thus offering the extra degrees of freedom typically needed in any gravitational modification [34]. Myrzakulov gravity can thus lead to a good phenomenology, being able to describe the Universe evolution at early and late times [35–39].

One basic question in modified gravities is the determination of the arbitrary function that enters in the theory. Although some general features can be deduced through theoretical considerations, such as the absence of ghosts and instabilities or the existence of Noether symmetries, the most powerful tool is the use of observational data [40–60]. Hence, in this work, we are interested in using expansion data such as supernovae type Ia data (SNIa), baryonic acoustic oscillations (BAOs), and Hubble cosmic chronometers (CC) observations, in order to impose constraints on Myrzakulov gravity. The plan of the work is the following. In Sec. II, we present Myrzakulov gravity and its cosmological applications. In Sec. III, we describe the various datasets and the involved statistical methods. Then, in Sec. IV, we preform our analysis, and we present the results, namely, the constraints on the various parameters. Finally, in Sec. V, we summarize and conclude.

II. MYRZAKULOV GRAVITY AND COSMOLOGY

In this section, we present a brief review of Myrzakulov gravity, or $F(R,T)$ gravity [34,35], extracting additionally the relevant cosmological equations.

A. Myrzakulov gravity

The central idea of this modified gravity is the modification of the underlying connection. In particular, it is known that, imposing a general connection $\omega^{a}{}_{bc}$, one defines the curvature and the torsion tensor, respectively, as [21]

$$R^{a}{}_{b\mu\nu} = \omega^{a}{}_{b\nu,\mu} - \omega^{a}{}_{b\mu,\nu} + \omega^{a}{}_{c\mu}\omega^{c}{}_{b\nu} - \omega^{a}{}_{c\nu}\omega^{c}{}_{b\mu}, \tag{2.1}$$

$$T^{a}{}_{\mu\nu} = e^{a}{}_{\nu,\mu} - e^{a}{}_{\mu,\nu} + \omega^{a}{}_{b\mu}e^{b}{}_{\nu} - \omega^{a}{}_{b\nu}e^{b}{}_{\mu}, \tag{2.2}$$

where $e_{a}{}^{\mu}\partial_{\mu}$ is the tetrad field related to the metric through $g_{\mu\nu} = \eta_{ab}e^{a}{}_{\mu}e^{b}{}_{\nu}$, where $\eta_{ab} = \mathrm{diag}(1,-1,-1,-1)$, with greek and latin indices denoting coordinate and tangent space, respectively, and where a comma denotes differentiation.

There are infinite connection choices. The Levi-Civita Γ_{abc} is the only connection that gives vanishing torsion, and from now on, we use the label "LC" to denote the curvature (Riemann) tensor corresponding to Γ_{abc}, namely, $R^{(\mathrm{LC})a}{}_{b\mu\nu} = \Gamma^{a}{}_{b\nu,\mu} - \Gamma^{a}{}_{b\mu,\nu} + \Gamma^{a}{}_{c\mu}\Gamma^{c}{}_{b\nu} - \Gamma^{a}{}_{c\nu}\Gamma^{c}{}_{b\mu}$. On the other hand, one can use the Weitzenböck connection $W^{\lambda}{}_{\mu\nu} = e_{a}{}^{\lambda}e^{a}{}_{\mu,\nu}$, which is curvatureless, leading only to torsion as $T^{(W)\lambda}{}_{\mu\nu} = W^{\lambda}{}_{\nu\mu} - W^{\lambda}{}_{\mu\nu}$ (we use the label "W" to denote quantities corresponding to $W^{\lambda}{}_{\mu\nu}$. From the above, it is implied that the Ricci scalar corresponding to the Levi-Civita connection is

$$R^{(\mathrm{LC})} = \eta^{ab}e_{a}{}^{\mu}e_{b}{}^{\nu}[\Gamma^{\lambda}{}_{\mu\nu,\lambda} - \Gamma^{\lambda}{}_{\mu\lambda,\nu} + \Gamma^{\rho}{}_{\mu\nu}\Gamma^{\lambda}{}_{\lambda\rho} - \Gamma^{\rho}{}_{\mu\lambda}\Gamma^{\lambda}{}_{\nu\rho}], \tag{2.3}$$

while the torsion scalar corresponding to the Weitzenböck connection is

$$\begin{aligned} T^{(W)} = {} & \frac{1}{4}(W^{\mu\lambda\nu} - W^{\mu\nu\lambda})(W_{\mu\lambda\nu} - W_{\mu\nu\lambda}) \\ & + \frac{1}{2}(W^{\mu\lambda\nu} - W^{\mu\nu\lambda})(W_{\lambda\mu\nu} - W_{\lambda\nu\mu}) \\ & - (W_{\nu}{}^{\mu\nu} - W_{\nu}{}^{\nu\mu})(W^{\lambda}{}_{\mu\lambda} - W^{\lambda}{}_{\lambda\mu}). \end{aligned} \tag{2.4}$$

As it is known, the former is used in the Lagrangian of general relativity and in all curvature-based modified gravities, e.g., in $F(R)$ gravity [8], while the latter is used in the Lagrangian of teleparallel equivalent of general relativity and in all torsion-modified gravities, e.g., in $F(T)$ gravity [6].

In Myrzakulov gravity, one uses a nonspecial connection which has nonzero curvature and torsion simultaneously [35]. Hence, the resulting theory will in general possess extra degrees of freedom, even if the imposed Lagrangian is simple, which is not the case of general relativity or of the teleparallel equivalent of general relativity that both have 2 degrees of freedom corresponding to the massless graviton. The action of the theory is

$$S = \int d^4x e\left[\frac{F(R,T)}{2\kappa^2} + L_m\right], \tag{2.5}$$

where $e = \det(e^{a}_{\mu}) = \sqrt{-g}$, $\kappa^2 = 8\pi G$ is the gravitational constant and where we have introduced the matter Lagrangian L_m, too, for completeness. Note that in the arbitrary function $F(R,T)$ the R and T are the curvature and torsion scalars corresponding to the nonspecial connection used, which read as [21]

$$T = \frac{1}{4}T^{\mu\nu\lambda}T_{\mu\nu\lambda} + \frac{1}{2}T^{\mu\nu\lambda}T_{\lambda\nu\mu} - T_{\nu}{}^{\nu\mu}T^{\lambda}{}_{\lambda\mu}, \tag{2.6}$$

$$R = R^{(\mathrm{LC})} + T - 2T_{\nu}{}^{\nu\mu}{}_{;\mu}, \tag{2.7}$$

where ; marks the covariant differentiation with respect to the Levi-Civita connection. Therefore, T depends on the tetrad field, its first derivative, and the connection, while R depends on the tetrad and its first derivative and on the connection and its first derivative, with an additional dependence on the second tetrad derivative due to the last term of (2.7). Thus, using (2.4), (2.6), and (2.7), we can finally write

$$T = T^{(W)} + v, \tag{2.8}$$

$$R = R^{(\mathrm{LC})} + u, \tag{2.9}$$

where v is a scalar depending on the tetrad, its first derivative, and the connection, while u is a scalar depending on the tetrad, its first and second derivatives, and the connection and its first derivative.

The quantities u and v quantify the effect of the specific but nonspecial imposed connection. In the case where this connection becomes the Levi-Civita one, then $u = 0$ and $v = -T^{(W)}$, and the above theory becomes the usual $F(R)$ gravity, which in turn coincides with general relativity under $F(R) = R$. On the other hand, in the case where the connection is the Weitzenböck one, then we have that $v = 0$ and $u = -R^{(\mathrm{LC})}$, and hence the theory coincides with $F(T)$ gravity, which in turn becomes the teleparallel equivalent of general relativity for $F(T) = T$.

B. Cosmology

Let us now apply the above into a cosmological framework and extract the corresponding equations that determine the Universe evolution. As it was shown in Ref. [35], in order to avoid complications related to the additional variation in terms of the connection, it proves convenient to apply a minisuperspace procedure. Hence, we apply the homogeneous and isotropic flat Friedmann-Robertson-Walker (FRW) geometry

$$ds^2 = dt^2 - a^2(t)\delta_{ij}dx^i dx^j, \tag{2.10}$$

which corresponds to the tetrad $e^a{}_\mu = \mathrm{diag}[1, a(t), a(t), a(t)]$, where $a(t)$ is the scale factor. In this case, one can easily find that $R^{(\mathrm{LC})} = 6(\frac{\ddot{a}}{a} + \frac{\dot{a}^2}{a^2})$ and $T^{(W)} = -6(\frac{\dot{a}^2}{a^2})$. Furthermore, we use the standard replacement $L_m = -\rho_m(a)$ [61–63]. Lastly, following the discussion on the dependence of u and v above, we consistently impose that $u = u(a, \dot{a}, \ddot{a})$ and $v = v(a, \dot{a})$.

In this work, we are interested in exploring the cosmological behavior that arises purely from the nonspecial connection of Myrzakulov gravity. Hence, we focus on the simplest case where the involved arbitrary function is trivial, namely, $F(R, T) = R + \lambda T$ with λ a dimensionless parameter (we omit the coupling coefficient of R since it can be absorbed into κ^2). Note that we do not consider an explicit cosmological constant term in the Lagrangian. Inserting the above minisuperspace expressions into the action (2.5), for this Lagrangian choice, we acquire $S = \int L dt$, where

$$L = \frac{3}{\kappa^2}[\lambda + 1]a\dot{a}^2 - \frac{a^3}{2\kappa^2}[u(a, \dot{a}, \ddot{a}) + \lambda v(a, \dot{a})] + a^3\rho_m(a). \tag{2.11}$$

Extracting the equations of motion for a, alongside the Hamiltonian constraint $\mathcal{H} = \dot{a}[\frac{\partial L}{\partial \dot{a}} - \frac{\partial}{\partial t}\frac{\partial L}{\partial \ddot{a}}] + \ddot{a}(\frac{\partial L}{\partial \ddot{a}}) - L = 0$, we finally acquire the Friedmann equations

$$3H^2 = \kappa^2(\rho_m + \rho_{de}) \tag{2.12}$$

$$2\dot{H} + 3H^2 = -\kappa^2(p_m + p_{de}), \tag{2.13}$$

where

$$\rho_{de} = \frac{1}{\kappa^2}\left[\frac{Ha}{2}(u_{\dot{a}} + v_{\dot{a}}\lambda) - \frac{1}{2}(u + \lambda v) + \frac{au_{\ddot{a}}}{2}(\dot{H} - 2H^2) - 3\lambda H^2\right] \tag{2.14}$$

$$p_{de} = -\frac{1}{\kappa^2}\left[\frac{Ha}{2}(u_{\dot{a}} + v_{\dot{a}}\lambda) - \frac{1}{2}(u + \lambda v) - \frac{a}{6}(u_a + \lambda v_a - \dot{u}_{\dot{a}} - \lambda\dot{v}_{\dot{a}}) - \frac{a}{2}(\dot{H} + 3H^2)u_{\ddot{a}} - Ha\dot{u}_{\ddot{a}} - \frac{a}{6}\ddot{u}_{\ddot{a}} - \lambda(2\dot{H} + 3H^2)\right], \tag{2.15}$$

with $H = \frac{\dot{a}}{a}$ the Hubble parameter, p_m the matter pressure, and the subscripts $a, \dot{a}, \ddot{a}$ denoting partial derivatives with respect to this argument. Hence, in the theory at hand, we obtain an effective dark energy sector which arises from the nonspecial connection. Additionally, given the matter conservation equation $\dot{\rho}_m + 3H(\rho_m + p_m) = 0$, we find

$$\dot{\rho}_{de} + 3H(\rho_{de} + p_{de}) = 0, \tag{2.16}$$

which implies that the effective dark energy sector is conserved.

The above Friedmann equations can efficiently describe the late-time acceleration. A first observation is that in the case where $\lambda = 0$, namely, in the case where the Lagrangian is just the curvature (nevertheless, the nonspecial connection leads to nonzero torsion, too), and for the choice $u = c_1\dot{a} - c_2$, with c_1, c_2 constants, we have $\rho_{de} = -p_{de} = \frac{c_2}{2\kappa^2} \equiv \Lambda$. Hence, the scenario at hand includes ΛCDM cosmology as a subcase, although we have not considered an explicit cosmological constant, since the cosmological constant arises effectively from the connection structure of the theory. Thus, we expect that a realistic model would be a deviation from the above scenario.

Finally, it proves convenient to introduce the deceleration parameter as

$$q = -1 - \frac{\dot{H}}{H^2}, \tag{2.17}$$

which quantifies the cosmic acceleration. Defining additionally the density parameters $\Omega_m = \kappa^2\rho_m/(3H^2)$ and

$\Omega_{de} = \kappa^2\rho_{de}/(3H^2)$, as well as the equation-of-state parameters $w_m \equiv p_m/\rho_m$ and $w_{de} \equiv p_{de}/\rho_{de}$, we can extract the useful expression

$$\frac{2q-1}{3} = \Omega_m w_m + \Omega_{de} w_{de}. \tag{2.18}$$

Hence, in the standard case of dust matter, namely, for $w_m \approx 0$, we obtain

$$w_{de} = \frac{2q-1}{3(1-\Omega_m)}. \tag{2.19}$$

This expression allows one to find the evolution of the dark energy equation-of-state parameter, knowing the solution of the Friedmann equations, or knowing the observable values of $H(z)$ (where z is the redshift defined through $1+z = a_0/a$ setting the current value of the scale factor to $a_0 = 1$).

In the following, we will focus to two models which can satisfy these features.

1. Model 1

Choosing $u = c_1\dot{a} - c_2$ and $v = c_3\dot{a} - c_4$, with c_3,c_4 constants, we obtain

$$3H^2 = \kappa^2(\rho_m + \rho_{de}) \tag{2.20}$$

$$2\dot{H} + 3H^2 = -\kappa^2(p_m + p_{de}), \tag{2.21}$$

with

$$\rho_{de} = \frac{1}{\kappa^2}[c - 3\lambda H^2] \tag{2.22}$$

$$p_{de} = -\frac{1}{\kappa^2}[c - \lambda(2\dot{H} + 3H^2)], \tag{2.23}$$

where $c \equiv c_2 + c_4$. Hence, in this scenario, the geometrical sector constitutes an effective dark energy sector with the above energy density and pressure and an equation-of-state parameter of the form

$$w_{de} = -1 + \frac{2\lambda\dot{H}}{c - 3\lambda H^2}. \tag{2.24}$$

Interestingly enough, we can see that w_{de} can be both larger or smaller than -1, and thus the effective dark energy can be quintessence-like or phantomlike.

This model has two parameters, namely, c and λ, but one of them can be eliminated using the present value of the matter density parameter Ω_{m0} (from now on, the subscript 0 denotes the current value of a quantity), since (2.20) at present gives

$$1 = \Omega_{m0} + \frac{c}{3H_0^2} - \lambda. \tag{2.25}$$

Additionally, the deceleration parameter (2.18), using (2.22) and (2.23), becomes

$$q(z) = -1 + \frac{2\Omega_{m0}(1+z)^3}{\Omega_{m0}(1+z)^3 + 2(1+\lambda-\Omega_{m0})}, \tag{2.26}$$

and thus its value at present is

$$q_0 = -1 + \frac{3\Omega_{m0}}{2(1+\lambda)}. \tag{2.27}$$

Comparing with the corresponding value of ΛCDM scenario, namely, $q_0^\Lambda = -1 + 3\Omega_{m0}/2$, we verify that for the special case of $\lambda = 0$ the two scenarios coincide, as mentioned above. Finally, note that from relation (2.26) we can calculate the transition redshift, namely, the redshift in which q transits from positive to negative and we have the onset of acceleration, finding

$$z_{\rm tr} = -1 + 2^{1/3}(1+\lambda-\Omega_{m0})^{1/3}\Omega_{m0}^{-1/3}. \tag{2.28}$$

2. Model 2

As a second example, let us consider a more general model with $u = c_1\frac{\dot{a}}{a}\ln\dot{a}$ and $v = s(a)\dot{a}$, with $s(a)$ an arbitrary function. In this case, Eqs. (2.14) and (2.15) give

$$3H^2 = \kappa^2(\rho_m + \rho_{de}) \tag{2.29}$$

$$2\dot{H} + 3H^2 = -\kappa^2(p_m + p_{de}), \tag{2.30}$$

with

$$\rho_{de} = \frac{1}{\kappa^2}\left[\frac{c_1}{2}H - 3\lambda H^2\right] \tag{2.31}$$

$$p_{de} = -\frac{1}{\kappa^2}\left[\frac{c_1}{2}H + \frac{c_1}{6}\frac{\dot{H}}{H} - \lambda(2\dot{H} + 3H^2)\right], \tag{2.32}$$

while

$$w_{de} = -1 + \frac{2\lambda\dot{H} - \frac{c_1}{6}\frac{\dot{H}}{H}}{\frac{c_1}{2}H - 3\lambda H^2}. \tag{2.33}$$

Similarly to the previous example, for this case, too, w_{de} can be quintessencelike or phantomlike.

This model has two parameters, namely, c_1 and λ, but one of them can be eliminated using Ω_{m0}, since (2.20) at present time leads to

$$1 = \Omega_{m0} + \frac{c_1}{6H_0} - \lambda. \tag{2.34}$$

The deceleration parameter (2.18) becomes

$$q(z) = -1 + \frac{\frac{3}{2}\Omega_{m0}(1+z)^3}{3(1-\Omega_{m0}+\lambda) + (1+\lambda)^{-1}[(1-\Omega_{m0}+\lambda)^2 + (1+\lambda)(1+z)^3\Omega_{m0}]^{1/2}}, \tag{2.35}$$

and its current value is

$$q_0 = -1 + \frac{\frac{3}{2}\Omega_{m0}}{3(1-\Omega_{m0}+\lambda) + (1+\lambda)^{-1}[(1-\Omega_{m0}+\lambda)^2 + (1+\lambda)\Omega_{m0}]^{1/2}}. \tag{2.36}$$

Finally, from relation (2.35), we can calculate the transition redshift as

$$\begin{aligned} z_{\rm tr} = -1 + &\frac{6^{1/3}(1+\lambda)^{-1/3}\Omega_{m0}^{-1/3}}{3} \\ &\cdot \{10 + 9\lambda(2+\lambda-\Omega_{m0}) - 9\Omega_{m0} \\ &- \sqrt{28 - 36\Omega_{m0} + 9[3\lambda(2+\lambda) - 4\lambda\Omega_{m0} + \Omega_{m0}^2]}\}^{1/3}. \end{aligned} \tag{2.37}$$

III. DATA AND METHODOLOGY

In this section, we describe the various datasets that are going to be used in our analysis and also the involved statistical methods. In particular, we will use data from direct measurements of the Hubble parameter, from SNIa, and from BAOs. Finally, we present various information criteria that offer information on the quality of the fit.

A. Cosmological probes

1. Direct measurements of the Hubble expansion

From the latest $H(z)$ dataset compilation available in Ref. [64], we use only data obtained from CCs. By using the differential age of passive evolving galaxies, one can measure the Hubble rate directly (see, e.g., Ref. [65] and references therein). These galaxies are massive galaxies that evolve "slowly" at certain intervals of the cosmic time, i.e., with small fraction of "new" stars. A striking advantage of the differential age of passive evolving galaxies is that the resulting measurement of the Hubble rate comes without any assumptions for the underlying cosmology, with the exception of imposed spatial flatness. Our study incorporates $N = 31$ measurements of the Hubble expansion in the redshift range $0.07 \lesssim z \lesssim 2.0$.

Here, the corresponding χ^2_H function reads

$$\chi^2_H(\phi^\nu) = \sum_{i=1}^{N} \frac{[H_i^{\rm obs} - H_{th}(z_i;\phi^\nu)]^2}{\sigma_i^2}, \tag{3.1}$$

where $H_i^{\rm obs}$ is the observed Hubble rate at redshift z_i and σ_i the corresponding uncertainty, while ϕ^ν is the statistical vector that contains the free parameters of the examined model.

2. Supernovae type Ia

The most common class of cosmological probes is the so-called standard candles. The latter are luminous extra-galactic astrophysical objects with observable features that are independent of the cosmic time. The most known standard candles and probably the most thoroughly studied are SNIa. In our analysis, we use the most recent SNIa dataset available, i.e., the binned Pantheon sample of Scolnic *et al.* [66]. The full dataset is approximated very efficiently with the binned $N = 40$ data points belonging to the redshift interval $0.01 \lesssim z \lesssim 1.6$. The corresponding χ^2 is

$$\chi^2_{\rm SNIa}(\phi^{\nu+1}) = \mu_{\rm SNIa}\mathbf{C}^{-1}_{\rm SNIa,cov}\mu^T_{\rm SNIa}, \tag{3.2}$$

where $\mu_{\rm SNIa} = \{\mu_1 - \mu_{\rm th}(z_1,\phi^\nu), \ldots, \mu_N - \mu_{\rm th}(z_N,\phi^\nu)\}$. The distance modulus reads as $\mu_i = \mu_{B,i} - \mathcal{M}$, with $\mu_{B,i}$ the apparent maximum magnitude for redshift z_i. Here, $\mathcal{M}$ is a hyperparameter [66] that quantifies uncertainties of various origins, such as astrophysical ones, a data-reduction pipeline, etc., and it is employed instead of the usage of α, β free parameters, in the context of "BEAMS with Bias Corrections" method [67]. The observed distance modulus is compared with the theoretical one, i.e.,

$$\mu_{\rm th} = 5\log\left(\frac{d_L(z;\phi^\nu)}{\rm Mpc}\right) + 25, \tag{3.3}$$

with

$$d_L(z;\phi^\nu) = c(1+z)\int_0^z \frac{dx}{H(x,\phi^\nu)} \tag{3.4}$$

the luminosity distance for flat FRW geometry. It must be noted that $\mathcal{M}$ and the normalized Hubble constant h are

degenerate in light of Pantheon dataset in an intrinsic way, as is usual in standard candles. Therefore, one should jointly employ other datasets in order to obtain meaningful information regarding the present value H_0.

3. Baryonic acoustic oscillations

Baryonic acoustic oscillations refer to the imprint left by relativistic sound waves in the early Universe, providing an observable to the late-time large scale structure. The main idea is to measure the aforementioned scale at different times (i.e., redshifts) and thus obtain $D_A(z)$ and $H(z)$. The acoustic length scale corresponds to the comoving distance that the sound waves could travel until the recombination z_* [68], namely,

$$r_d = \int_{z_*}^{\infty} \frac{c_s(z)}{H(z)}. \tag{3.5}$$

For the concordance model, the sound speed, c_s, is given from an analytical expression. However, for the models considered here, there is not such an expression; therefore, the scale r_d will be addressed as a free parameter. Furthermore, distances of different objects along the line of sight correspond to different redshifts and thus depend on the combination $H(z)r_d$, while distances transverse to the line of sight are related with the combination $D_A(z)/r_d$.

Employing large samples of tracers, (i.e., galaxies), one can detect by statistical means the BAO peak (for details, see Ref. [69] and references therein). To achieve this, it is required to impose an underlying cosmology, and hence the method is not model independent. However, the differences that may infiltrate at the final data products are much less than the statistical errors, and in most cases, the data points are calibrated with the quantity $r_{d,\mathrm{fid}}/r_d$. In this work, we employ the BAOs dataset used by Ref. [70], that consists of $N = 11$ data points in the redshift range $0.106 \lesssim z \lesssim 2.36$. The relevant χ^2 function reads as

$$\chi^2_{\mathrm{BAO}}(\phi^{\nu+1}) = \mathbf{s} C^{-1}_{\mathrm{cov}} \mathbf{s}^T + \sum_{i=8}^{N} \frac{[T(z_i;\phi^\nu) - T_i^{\mathrm{obs}}]^2}{\sigma_i^2}, \tag{3.6}$$

with C^{-1}_{cov} the inverse of the covariance matrix of the first six measurements available in Ref. [70]. The vector $\mathbf{s}$ has as elements the s_i, given as $s_i = d_m - d_i^{\mathrm{obs}} r_d/r_{d,\mathrm{fid}}$ for odd i and $s_i = H(z_i;\phi^\nu) - H_i^{\mathrm{obs}} r_{d,\mathrm{fid}}/r_d$ for even i. In all cases, $r_{d,\mathrm{fid}} = 147.78$. Furthermore, for $i \in \{8,9\}$, $T(z_i;\phi^\nu) = D_v(z_i;\phi^\nu)$, $T_i^{\mathrm{obs}} = D_{v,i}^{\mathrm{obs}} r_d/r_{d,\mathrm{fid}}$, with $r_{\mathrm{fid},8} = 148.69$ Mpc and $r_{\mathrm{fid},9} = 147.66$ Mpc, respectively. For $i = 10$, $T(z_i;\phi^\nu) = cH(z_i;\phi^\nu)^{-0.7} D_m(z_i;\phi^\nu)^{0.3}/r_d$ and for $i = 11$, $T(z_i;\phi^\nu) = cH(z_i;\phi^\nu)^{-1} r_d$. Finally, in the expressions above, the following quantities have been used:

$$D_M(z_i;\phi^\nu) = \frac{D_L(z_i;\phi^\nu)}{1+z}, \tag{3.7a}$$

$$D_A(z_i;\phi^\nu) = \frac{D_L(z_i;\phi^\nu)}{(1+z)^2}, \tag{3.7b}$$

$$D_V(z;\phi^\nu) = \left[\frac{cD_A(z;\phi^\nu)^2 z(1+z)^2}{H(z;\phi^\nu)}\right]^{1/3}. \tag{3.7c}$$

4. Big bang nucleosynthesis

Any cosmological scenario arising from modified gravity should preserve the standard thermal history of the Universe. Hence, a basic and rough condition is applicable in the form of an extra prior. Specifically, we require that the following inequality holds [71–73],

$$\frac{(H_i(z_{\mathrm{BBN}};\phi^\nu) - H_\Lambda(z_{\mathrm{BBN}};\Omega_{m0}))^2}{H_\Lambda(z_{\mathrm{BBN}};\Omega_{m0})^2} < 0.1, \tag{3.8}$$

where $z_{\mathrm{BBN}} \sim 10^9$. For the fiducial ΛCDM cosmology, namely, H_Λ, we employ the parameter values from Planck [74].

5. Joint likelihood analysis

To obtain the joint constraints on the cosmological parameters from the aforementioned cosmological probes, we introduce the total likelihood function as

$$\mathcal{L}_{\mathrm{tot}}(\phi^k) = \mathcal{L}_{\mathrm{SNIa}} \times \mathcal{L}_H \times \mathcal{L}_{\mathrm{BAO}}. \tag{3.9}$$

It is easy to deduce that relevant χ^2_{tot} is given as

$$\chi^2_{\mathrm{tot}}(\phi^k) = \chi^2_{\mathrm{SNIa}} + \chi^2_H + \chi^2_{\mathrm{BAO}}. \tag{3.10}$$

The involved statistical vector has k components, i.e., the ν parameters of the scenario at hand plus ν_{hyp} hyperparameters from the imposed datasets, namely, $k = \nu + \nu_{\mathrm{hyp}}$. Hence, the vector containing the free parameters of the scenarios at hand is $\phi^k = \{\Omega_{m0}, h, \lambda, \mathcal{M}, r_d\}$. Note, however, that from a statistical point of view there is no distinction between the intrinsic hyperparameters of a given dataset and the free parameters of a cosmological scenario.

Finally, for the likelihood maximization, we use an affine-invariant Markov chain Monte Carlo (MCMC) sampler [75], obtained in the PYTHON package EMCEE [76]. We use 1000 chains (walkers) and 3500 steps (states). As a prior, we employ first the conditions $0.0 < \Omega_{m0} < 1$, $0.60 < h < 0.90$, $-19.9 < M < -18.0$, $-0.9 < \lambda < 2.8$, and $135 < r_d < 160$ and second the big bang nucleosynthesis (BBN) constraint described above. Lastly, the convergence of the MCMC algorithm is verified with autocorrelation time implementation, and moreover for completeness, the Gelman-Rubin criterion is calculated.

B. Information criteria and model selection

As a last step, we present the standard ways in order to compare a set of cosmological scenarios, namely, we apply the Akaike Information Criterion (AIC) [77], the Bayesian Information Criterion (BIC) [78], and the Deviance Information Criterion (DIC) [79]. Moreover, we present the standard $\chi^2_{\rm min}/{\rm dof}$, where "dof" stands for degrees of freedom, usually defined as the number of the used data points minus the number of fitted parameters. In our case, this gives dof $= 77$. Nevertheless, $\chi^2_{\rm min}/{\rm dof}$ should be used for illustrative purposes, as the degrees of freedom might be ambiguous for nonlinear (in terms of the free parameters) models. [80].

The AIC criterion is based on information theory, and it is an asymptotically unbiased estimator of the Kullback-Leibler information. Under the standard assumption of Gaussian errors, the corresponding estimator for the AIC criterion reads [81,82]

$$\mathrm{AIC} = -2\ln(\mathcal{L}_{\rm max}) + 2k + \frac{2k(k+1)}{N_{\rm tot}-k-1}, \tag{3.11}$$

with $\mathcal{L}_{\rm max}$ the maximum likelihood of the dataset(s) under consideration and $N_{\rm tot}$ the total data points number. It is apparent that for $N_{\rm tot} \gg 1$ this expression gives the original AIC version, namely, $\mathrm{AIC} \simeq -2\ln(\mathcal{L}_{\rm max}) + 2k$. As it is discussed in Ref. [83], it is considered as best practise to use the modified AIC criterion.

The BIC criterion is a Bayesian evidence estimator, and it is written as [81–83]

$$\mathrm{BIC} = -2\ln(\mathcal{L}_{\rm max}) + k log(N_{\rm tot}). \tag{3.12}$$

Finally, the DIC criterion employs both Bayesian statistics and information theory concepts [79], and it is expressed as [83]

$$\mathrm{DIC} = D(\overline{\phi^k}) + 2C_B. \tag{3.13}$$

The quantity C_B is the Bayesian complexity $C_B = \overline{D(\phi^k)} - D(\overline{\phi^k})$, where overlines imply the standard mean value. Moreover, $D(\phi^k)$ is the Bayesian Deviation, which can be expressed as $D(\phi^k) = -2\ln[\mathcal{L}(\phi^k)]$ in the case of exponential class of distributions. It is closely related to the number of effective degrees of freedom [79], which is actually the number of parameters that affect the fitting. In a less strict manner, it could be considered as a measure of the "spread" of the likelihood.

In contrast with AIC and BIC criteria, instead of using just the best fit likelihood, DIC uses the whole sample. Furthermore, AIC and BIC count and penalize all the involved parameters, while DIC penalizes only the number of parameters that contribute to the fit in an actual way. Finally, an additional appealing feature of DIC criterion is that its calculation is computationally light under the MCMC samples.

Given a set of scenarios that describe the same class of phenomena, our problem is to sort the models according to their fitting efficiency in the context of the available data. We employ the aforementioned three information criteria (IC), and we calculate the relative difference of the IC value for the given set of models, $\Delta\mathrm{IC}_{\rm model} = \mathrm{IC}_{\rm model} - \mathrm{IC}_{\rm min}$, where the $\mathrm{IC}_{\rm min}$ is the minimum IC value inside the competing models set. To qualify each model in terms of its relevant adequacy, we apply the Jeffreys scale [84]. Specifically, the condition $\Delta\mathrm{IC} \leq 2$ implies statistical compatibility with the most favored model by the data, while the condition $2 < \Delta\mathrm{IC} < 6$ corresponds to middle tension between the two models, and lastly the condition $\Delta\mathrm{IC} \geq 10$ implies strong tension.

IV. RESULTS

In this section, we proceed to the observational analysis of Myrzakulov gravity using the datasets and the methods described above. Note that the free parameters of the aforementioned models are Ω_{m0}, h, and λ, while for the case of the concordance cosmology they are Ω_{m0} and h. For convenience, we summarize the obtained results in Table I. Additionally, in Figs. 1 and 2, we present the corresponding contour plots for model 1 and model 2, respectively. For comparison and benchmark, we also analyzed the concordance model, namely, ΛCDM.

As we can see, according to the combined analysis of CC +SNIa+BAO data, we acquire approximately 1σ compatibility in all cases. The dimensionless parameter λ is constrained to an interval around 0, that includes ΛCDM paradigm, which was expected since as we discussed above a realistic modified gravity should be a small deviation

TABLE I. Observational constraints and the corresponding $\chi^2_{\rm min}$, as well as $\chi^2_{\rm min}/{\rm dof}$ (where "dof" stands for degrees of freedom, in our case dof $= 77$), for the two Myrzakulov gravity models, presented previously, using CC/Pantheon/BAO datasets. To allow direct comparison, the concordance flat ΛCDM model is also analyzed, giving results very similar with the corresponding ones of Ref. [85].

Model	Ω_{m0}	h	λ	r_d	$\mathcal{M}$	$\chi^2_{\rm min}$	$\chi^2_{\rm min}/{\rm dof}$
1	$0.425^{+0.107}_{-0.146}$	$0.691^{+0.016}_{-0.017}$	$0.491^{+0.387}_{-0.533}$	$146.20^{+2.55}_{-3.41}$	$-19.382^{+0.051}_{-0.052}$	61.93	0.8043
2	$0.339^{+0.093}_{-0.122}$	$0.679^{+0.016}_{-0.016}$	$0.537^{+0.403}_{-0.550}$	$146.60^{+3.57}_{-3.44}$	$-19.396^{+0.051}_{-0.052}$	63.53	0.8251
ΛCDM	$0.292^{+0.015}_{-0.014}$	$0.692^{+0.017}_{-0.017}$	⋯	$145.87^{+3.53}_{-3.38}$	$-19.377^{+0.051}_{-0.052}$	61.73	0.7914

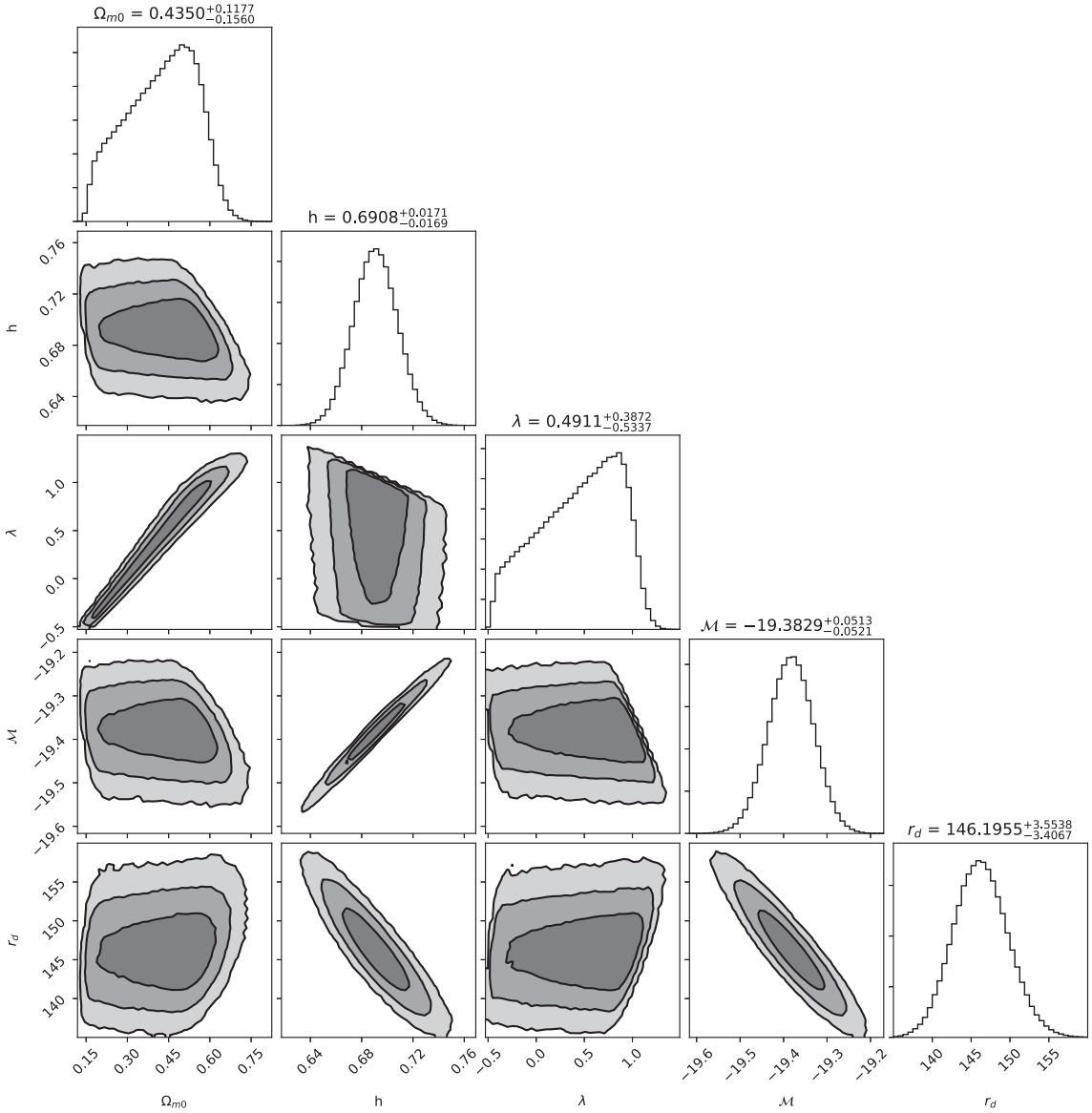

FIG. 1. The 1σ, 2σ, and 3σ likelihood contours for model 1 of (2.22) and (2.23), for all possible two-dimensional subsets of the parameter space $(\Omega_{m0}, h, \lambda, \mathcal{M}, r_d)$. Moreover, we present the mean parameter values within the 1σ area of the MCMC chain. We have performed a joint analysis of CC + SNIa + BAO data.

from general relativity. Nevertheless, note that in both model 1 and model 2 the λ contours are slightly shifted toward positive values. We mention that having the likelihood contours for the parameter λ allows us to extract the constraints on the parameter c through expression (2.25) for model 1 and on the parameter c_1 through (2.34) for model 2. In particular, for the 1σ region for model 1, we obtain $c = 1.550^{+0.828}_{-0.876}$, while for model 2, we find $c_1 = 4.94^{+2.28}_{-2.75}$.

Concerning the values of Ω_{m0}, we observe that model 1 gives a rather large value, due to the degeneracy with λ, while for model 2, this is not the case. Concerning the Hubble constant h, for model 1, we find that $0.690^{+0.016}_{-0.017}$, while for model 2, we obtain $0.679^{+0.016}_{-0.016}$. This implies that the obtained values for the present Hubble parameter H_0 are in between the Planck estimation $H_0 = 67.36 \pm 0.54$ km/s/Mpc [74] and the local estimation $H_0 = 73.24 \pm 1.74$ km/s/Mpc [86], although closer to the former. In addition, the extracted H_0 value for both models is consistent with other astrophysical inferences of Hubble constant, i.e., $H_0 = 67.4^{+4.1}_{-3.2}$ km s^{-1} Mpc^{-1} [87], and $H_0 = 69.6 \pm 2.5$ km s^{-1} Mpc^{-1} [88]. It is interesting to note that results in this range have been supported for about a decade now, among others references in Refs. [89–95].

To provide a more complete and transparent picture, we use the obtained allowed parameter values in order to

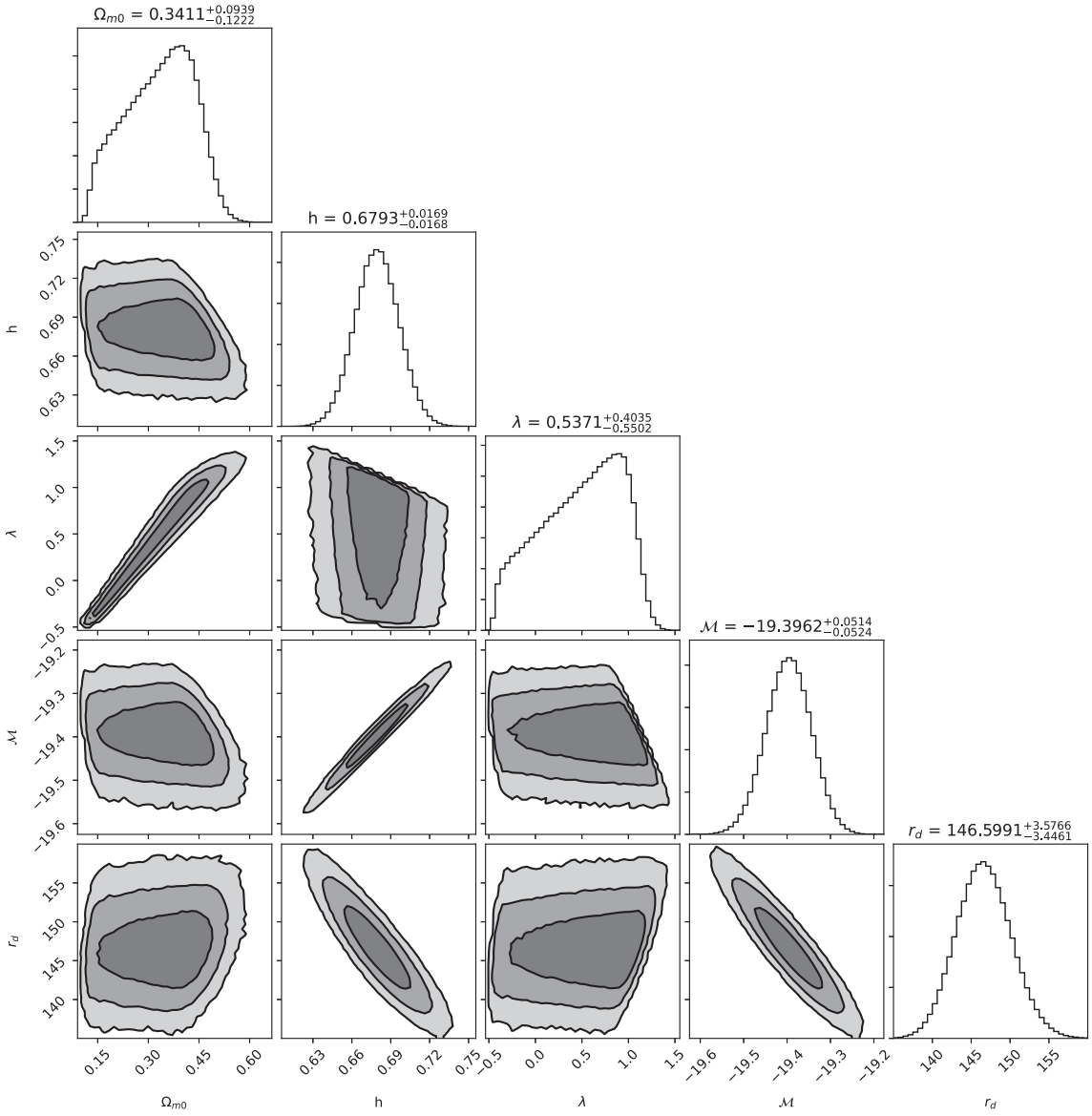

FIG. 2. The 1σ, 2σ, and 3σ likelihood contours for model 2 of (2.31) and (2.32), for all possible two-dimensional subsets of the parameter space $(\Omega_{m0}, h, \lambda, \mathcal{M}, r_d)$. Moreover, we present the mean parameter values within the 1σ area of the MCMC chain. We have performed a joint analysis of CC + SNIa + BAO data.

extract the resulting $H(z)$. In Figs. 3 and 4, we present the reconstructed mean $H(z)/(z+1)$ as a function of the redshift, alongside the allowed curves for the 1σ allowed model parameters presented above, for model 1 and model 2, respectively. These graphs are quite similar to the corresponding ones for quintessence models (ϕCDM) of Ref. [96].

As a next step, we investigate of the evolution of the dark energy equation-of-state parameter. In particular, having obtained the allowed parameter values at 1σ confidence level, we can use them in order to extract the resulting $w_{de}(z)$ behavior given by (2.19), with the deceleration parameter given by (2.26) for model 1 and by (2.35) for model 2.

In Fig. 5, we depict the reconstructed mean $w_{de}(z)$ (red curve) for model 1, alongside the allowed curves for the 1σ allowed model parameters presented above. As we observe, the corresponding behavior is very close to ΛCDM scenario for every parameter values. Similarly, in Fig. 6, we present the corresponding graph for model 2. In this case, the scenario resembles ΛCDM at low redshifts; however, at earlier times, the mean curve, as well as many of the "individual" curves, present a deviation, since this is allowed by the used datasets. In particular, for some parameter choices, the dark energy pressure at a particular redshift diverges and changes sign, and thus the $w_{de}(z)$ transits on the other side of the phantom divide. Such energy conditions violations are common in modified gravity theories, and

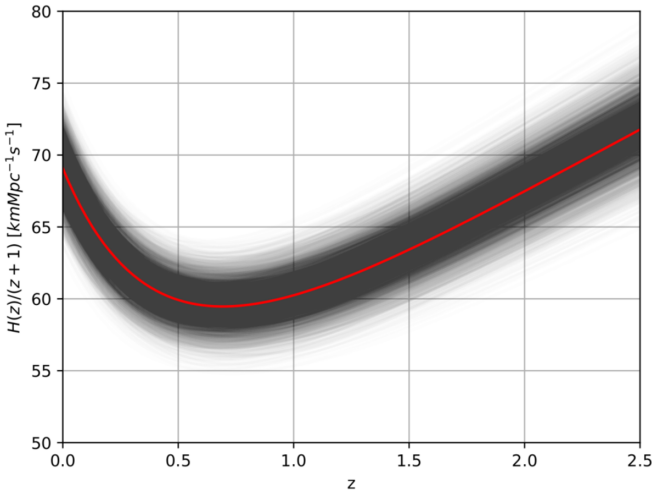

FIG. 3. The reconstruction of the $H(z)/(z+1)$ as a function of the redshift for model 1, arisen from (2.20) and (2.22). We resampled the chains produced by emcee taking 6000 samples, and we plot all the obtained curves, alongside the curve corresponding to the best fit of the parameters (red curve).

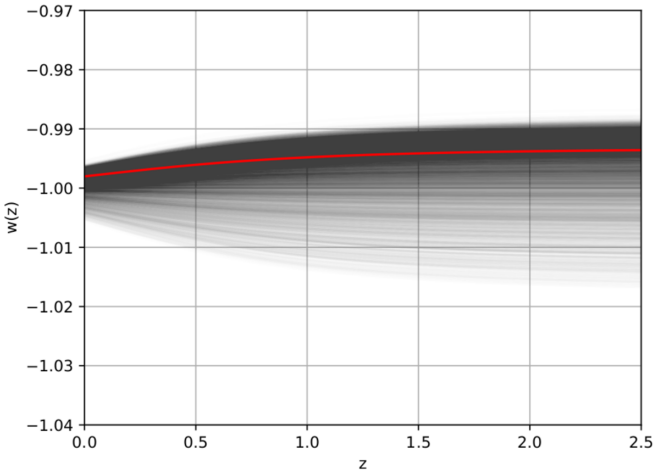

FIG. 5. The reconstruction of the effective dark energy equation-of-state parameter $w_{de}(z)$ as a function of the redshift for model 1 given by (2.24). We resampled the chains produced by EMCEE taking 6000 samples, and we plot all the obtained $w_{de}(z)$ curves, alongside the curve corresponding to the best fit of the parameters (red curve).

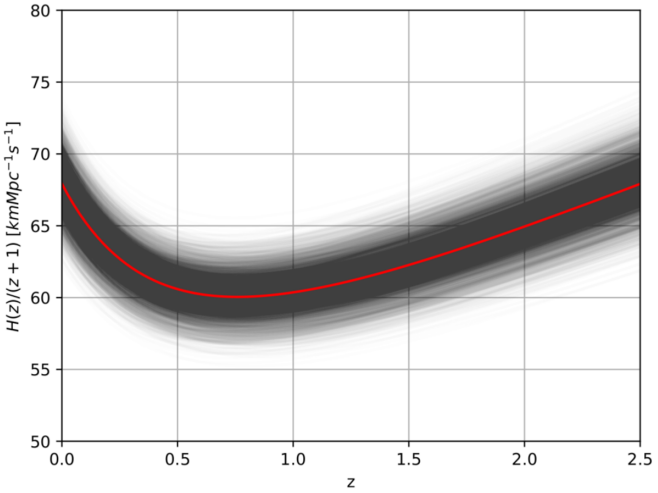

FIG. 4. The reconstruction of the $H(z)/(z+1)$ as a function of the redshift for model 2, arisen from (2.29) and (2.31). We resampled the chains produced by emcee taking 6000 samples, and we plot all the obtained curves, alongside the curve corresponding to the best fit of the parameters (red curve).

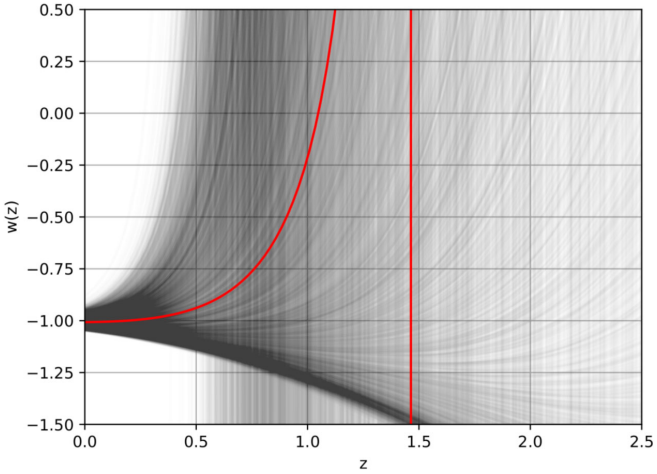

FIG. 6. The reconstruction of the effective dark energy equation-of-state parameter $w_{de}(z)$ as a function of the redshift for model 2 given by (2.33). We resampled the chains produced by EMCEE taking 6000 samples, and we plot all the obtained $w_{de}(z)$ curves, alongside the curve corresponding to the best fit of the parameters (red curve). The overpopulated area at the bottom corresponds to a peak within 1σ area; nevertheless, since we extract the median value of each parameter within 1σ as the best fit, the "best" $w_{de}(z)$ curve differs.

actually they can lead to interesting cosmological phenomenology. Note that the observable quantities (the Hubble function and its derivatives, the density parameters, etc.) remain finite. However, we mention that a significant subset of the curves, i.e., a large region of the parameter space of the model, does not exhibit such a behavior, and the individual obtained curves resemble the ΛCDM evolution.

Furthermore, we proceed to the reconstruction of the deceleration parameter using random sampling of the obtained chains. Concerning the current value q_0, for model 1 using (2.27), we obtain $q_0 = -0.561^{+0.022}_{-0.021}$, while for model 2 using (2.36), we acquire $q_0 = -0.880^{+0.010}_{-0.009}$. These are in agreement with the values obtained using other datasets, such as supernovae, quasars, and gamma-ray bursts by means of model-independent techniques [97].

Additionally, we calculate the transition redshift, for the two models, using relations (2.28) and (2.37), respectively. For model 1, we find $z_{\mathrm{tr},1} = 0.36^{+0.10}_{-0.18}$, while for model 2, we acquire $z_{\mathrm{tr},2} = 0.74^{+0.07}_{-0.14}$. It is of interest to compare

TABLE II. The information criteria AIC, BIC, and DIC for the examined cosmological models, alongside the relative difference from the best-fitted model $\Delta\mathrm{IC} \equiv \mathrm{IC} - \mathrm{IC}_{\mathrm{min}}$.

Model	AIC	ΔAIC	BIC	ΔBIC	DIC	ΔDIC
1	72.7234	2.4757	83.9675	4.6124	69.6728	0.0007
2	74.3204	4.0727	85.5645	6.2094	71.3725	1.7004
ΛCDM	70.2477	0	79.3551	0	69.6721	0

the aforementioned values with $z_{\mathrm{tr},A} = 0.72 \pm 0.05$ [96] and $z_{\mathrm{tr},B} = 0.64^{+0.12}_{-0.09}$ [98]. For model 1, we observe mild compatibility within approximately 3.5σ and within approximately 3σ with "A" and "B" results, respectively. On the other hand, for the case of model 2, we report 1σ compatibility with both results. These results act as an additional verification check of the examined models.

We close this analysis with the examination of the statistical significance of our fitting results, applying the AIC, BIC, and DIC information criteria described in Sec. III B. We summarize our results in Table II. As we observe, model 1 is statistically equivalent with ΛCDM paradigm, and especially the combined and more complete DIC criterion gives an almost equal value. Additionally, model 2 also presents a very good fitting behavior, and according to DIC, it is also statistically equivalent with ΛCDM paradigm, which is an interesting result since model 2 does not contain ΛCDM scenario as a limit for any parameter value.

V. CONCLUSIONS

In this work, we have used observational data from SNIa Pantheon sample, from BAOs, and from cosmic chronometers measurements of the Hubble parameter, alongside arguments from BBN, in order to extract constraints on Myrzakulov $F(R,T)$ gravity. This is a connection-based theory belonging to the Riemann-Cartan subclass, that uses a specific but nonspecial connection, which then leads to extra degrees of freedom. One introduces a parametrization that quantifies the deviation of torsion and curvature scalars form their values corresponding to the special Levi-Civita and Weitzenböck connections and then constructs various models by assuming specific forms for the involved functions. In all models, one obtains an effective dark energy sector of geometrical origin.

We considered two specific models, which are known to lead to interesting phenomenology. Our analysis shows that both models are capable of describing adequately the imposed datasets, namely, CC+SNIa+BAO ones, obtaining approximately 1σ compatibility in all cases. Concerning model 1, which includes ΛCDM paradigm as a particular limit, we found a relatively large value for Ω_{m0} and a value for h in between the Planck and local estimation, although closer to the former. For the dimensionless parameter λ, we found that it is constrained to an interval around 0, which corresponds to ΛCDM scenario; however, the corresponding contours are slightly shifted toward positive values. In the case of model 2, we found smaller Ω_{m0} and h, while λ is again constrained around 0 with favored positive values.

Additionally, we used the obtained posterior distribution of the parameters at 1σ confidence level, and we reconstructed the Hubble function as a function of the redshift. As we showed, the obtained graphs for $H(z)/(z+1)$ are in very good agreement with observations. Furthermore, we reconstructed the induced dark energy equation-of-state parameter as a function of the redshift. As we saw, for model 1, $w_{de}(z)$ is very close to ΛCDM scenario, while for model 2, it resembles ΛCDM at low redshifts; however, at earlier times, deviations are allowed.

Finally, applying the AIC, BIC, and the combined DIC criteria, we deduced that both model 1 and model 2 present a very efficient fitting behavior and are statistically equivalent with ΛCDM cosmology. This is an interesting result since model 2 does not contain ΛCDM scenario as a limit for any parameter value.

In summary, Myrzakulov $F(R,T)$ gravity is in agreement with cosmological data, and it could serve as a candidate for the description of nature. Nevertheless, one should also investigate the theory at the perturbation level and confront it with perturbation-related data, i.e., $f\sigma_8$. Such an analysis, although both interesting and necessary, lies beyond the scope of the present work, and it is left for a future project.

[1] K. A. Olive, Inflation, Phys. Rep. **190**, 307 (1990).
[2] N. Bartolo, E. Komatsu, S. Matarrese, and A. Riotto, Non-Gaussianity from inflation: Theory and observations, Phys. Rep. **402**, 103 (2004).
[3] E. J. Copeland, M. Sami, and S. Tsujikawa, Dynamics of dark energy, Int. J. Mod. Phys. D **15**, 1753 (2006).
[4] Y.-F. Cai, E. N. Saridakis, M. R. Setare, and J.-Q. Xia, Quintom Cosmology: Theoretical implications and observations, Phys. Rep. **493**, 1 (2010).
[5] S. Capozziello and M. De Laurentis, Extended theories of gravity, Phys. Rep. **509**, 167 (2011).
[6] Y. F. Cai, S. Capozziello, M. De Laurentis, and E. N. Saridakis, $f(T)$ teleparallel gravity and cosmology, Rep. Prog. Phys. **79**, 106901 (2016).
[7] P. Brax, C. van de Bruck, and A. C. Davis, Brane world cosmology, Rep. Prog. Phys. **67**, 2183 (2004).
[8] A. De Felice and S. Tsujikawa, $f(R)$ theories, Living Rev. Relativity **13**, 3 (2010).

[9] S. Nojiri and S. D. Odintsov, Unified cosmic history in modified gravity: From $f(R)$ theory to Lorentz non-invariant models, Phys. Rep. **505**, 59 (2011).
[10] S. Nojiri and S. D. Odintsov, Modified Gauss-Bonnet theory as gravitational alternative for dark energy, Phys. Lett. B **631**, 1 (2005).
[11] A. De Felice and S. Tsujikawa, Construction of cosmologically viable f(G) dark energy models, Phys. Lett. B **675**, 1 (2009).
[12] D. Lovelock, The Einstein tensor and its generalizations, J. Math. Phys. (N.Y.) **12**, 498 (1971).
[13] N. Deruelle and L. Farina-Busto, The Lovelock gravitational field equations in cosmology, Phys. Rev. D **41**, 3696 (1990).
[14] G. W. Horndeski, Second-order scalar-tensor field equations in a four-dimensional space, Int. J. Theor. Phys. **10**, 363 (1974).
[15] A. Nicolis, R. Rattazzi, and E. Trincherini, The Galileon as a local modification of gravity, Phys. Rev. D **79**, 064036 (2009).
[16] C. Deffayet, G. Esposito-Farese, and A. Vikman, Covariant Galileon, Phys. Rev. D **79**, 084003 (2009).
[17] R. Aldrovandi and J. G. Pereira, *Teleparallel Gravity: An Introduction* (Springer, Dordrecht, 2013).
[18] J. W. Maluf, The teleparallel equivalent of general relativity, Ann. Phys. (Amsterdam) **525**, 339 (2013).
[19] R. Ferraro and F. Fiorini, Modified teleparallel gravity: Inflation without inflaton, Phys. Rev. D **75**, 084031 (2007).
[20] E. V. Linder, Einstein's other gravity and the acceleration of the universe, Phys. Rev. D **81**, 127301 (2010).
[21] G. Kofinas and E. N. Saridakis, Teleparallel equivalent of Gauss-Bonnet gravity and its modifications, Phys. Rev. D **90**, 084044 (2014).
[22] C.-Q. Geng, C.-C. Lee, E. N. Saridakis, and Y.-P. Wu, Teleparallel dark energy, Phys. Lett. B **704**, 384 (2011).
[23] M. Hohmann, L. Järv, and U. Ualikhanova, Covariant formulation of scalar-torsion gravity, Phys. Rev. D **97**, 104011 (2018).
[24] F. W. Hehl, J. D. McCrea, E. W. Mielke, and Y. Ne'eman, Metric affine gauge theory of gravity: Field equations, Noether identities, world spinors, and breaking of dilation invariance, Phys. Rep. **258**, 1 (1995).
[25] J. B. Jimenez, A. Golovnev, M. Karciauskas, and T. S. Koivisto, The Bimetric variational principle for General Relativity, Phys. Rev. D **86**, 084024 (2012).
[26] N. Tamanini, Variational approach to gravitational theories with two independent connections, Phys. Rev. D **86**, 024004 (2012).
[27] G. Y. Bogoslovsky and H. F. Goenner, Finslerian spaces possessing local relativistic symmetry, Gen. Relativ. Gravit. **31**, 1565 (1999).
[28] N. E. Mavromatos, S. Sarkar, and A. Vergou, Stringy spacetime foam, Finsler-like metrics and dark matter relics, Phys. Lett. B **696**, 300 (2011).
[29] S. Basilakos, A. P. Kouretsis, E. N. Saridakis, and P. Stavrinos, Resembling dark energy and modified gravity with Finsler-Randers cosmology, Phys. Rev. D **88**, 123510 (2013).
[30] A. P. Kouretsis, M. Stathakopoulos, and P. C. Stavrinos, Covariant kinematics and gravitational bounce in Finsler space-times, Phys. Rev. D **86**, 124025 (2012).
[31] A. Triantafyllopoulos and P. C. Stavrinos, Weak field equations and generalized FRW cosmology on the tangent Lorentz bundle, Classical Quantum Gravity **35**, 085011 (2018).
[32] S. Ikeda, E. N. Saridakis, P. C. Stavrinos, and A. Triantafyllopoulos, Cosmology of Lorentz fiber-bundle induced scalar-tensor theories, Phys. Rev. D **100**, 124035 (2019).
[33] A. Conroy and T. Koivisto, The spectrum of symmetric teleparallel gravity, Eur. Phys. J. C **78**, 923 (2018).
[34] R. Myrzakulov, FRW cosmology in F(R,T) gravity, Eur. Phys. J. C **72**, 2203 (2012).
[35] E. N. Saridakis, S. Myrzakul, K. Myrzakulov, and K. Yerzhanov, Cosmological applications of $F(R,T)$ gravity with dynamical curvature and torsion, Phys. Rev. D **102**, 023525 (2020).
[36] M. Jamil, D. Momeni, M. Raza, and R. Myrzakulov, Reconstruction of some cosmological models in f(R,T) gravity, Eur. Phys. J. C **72**, 1999 (2012).
[37] M. Sharif, S. Rani, and R. Myrzakulov, Analysis of $F(R,T)$ gravity models through energy conditions, Eur. Phys. J. Plus **128**, 123 (2013).
[38] S. Capozziello, M. De Laurentis, and R. Myrzakulov, Noether Symmetry Approach for teleparallel-curvature cosmology, Int. J. Geom. Methods Mod. Phys. **12**, 1550095 (2015).
[39] P. Feola, X. J. Forteza, S. Capozziello, R. Cianci, and S. Vignolo, The mass-radius relation for neutron stars in $f(R) = R + \alpha R^2$ gravity: A comparison between purely metric and torsion formulations, Phys. Rev. D **101**, 044037 (2020).
[40] B. Feng, X. L. Wang, and X. M. Zhang, Dark energy constraints from the cosmic age and supernova, Phys. Lett. B **607**, 35 (2005).
[41] G. Olivares, F. Atrio-Barandela, and D. Pavon, Observational constraints on interacting quintessence models, Phys. Rev. D **71**, 063523 (2005).
[42] S. Capozziello, V. F. Cardone, E. Elizalde, S. Nojiri, and S. D. Odintsov, Observational constraints on dark energy with generalized equations of state, Phys. Rev. D **73**, 043512 (2006).
[43] R. Maartens and E. Majerotto, Observational constraints on self-accelerating cosmology, Phys. Rev. D **74**, 023004 (2006).
[44] R. Lazkoz, R. Maartens, and E. Majerotto, Observational constraints on phantom-like braneworld cosmologies, Phys. Rev. D **74**, 083510 (2006).
[45] W. M. Wood-Vasey *et al.* (ESSENCE Collaboration), Observational constraints on the nature of the dark energy: First cosmological results from the ESSENCE supernova survey, Astrophys. J. **666**, 694 (2007).
[46] X. Zhang and F. Q. Wu, Constraints on holographic dark energy from latest supernovae, galaxy clustering, and cosmic microwave background anisotropy observations, Phys. Rev. D **76**, 023502 (2007).
[47] S. Tsujikawa, Observational signatures of $f(R)$ dark energy models that satisfy cosmological and local gravity constraints, Phys. Rev. D **77**, 023507 (2008).

[48] S. Basilakos, M. Plionis, and J. Solà, Hubble expansion & structure formation in time varying vacuum models, Phys. Rev. D **80**, 083511 (2009).
[49] S. Dutta and E. N. Saridakis, Overall observational constraints on the running parameter λ of Horava-Lifshitz gravity, J. Cosmol. Astropart. Phys. 05 (2010) 013.
[50] S. Nesseris, A. De Felice, and S. Tsujikawa, Observational constraints on Galileon cosmology, Phys. Rev. D **82**, 124054 (2010).
[51] C. Q. Geng, C. C. Lee, and E. N. Saridakis, Observational constraints on teleparallel dark energy, J. Cosmol. Astropart. Phys. 01 (2012) 002.
[52] S. Basilakos, S. Nesseris, and L. Perivolaropoulos, Observational constraints on viable $f(R)$ parametrizations with geometrical and dynamical probes, Phys. Rev. D **87**, 123529 (2013).
[53] S. Basilakos and J. Solà, Growth index of matter perturbations in running vacuum models, Phys. Rev. D **92**, 123501 (2015).
[54] W. Yang, S. Pan, E. Di Valentino, E. N. Saridakis, and S. Chakraborty, Observational constraints on one-parameter dynamical dark-energy parametrizations and the H_0 tension, Phys. Rev. D **99**, 043543 (2019).
[55] F. K. Anagnostopoulos, S. Basilakos, and E. N. Saridakis, Bayesian analysis of $f(T)$ gravity using $f\sigma_8$ data, Phys. Rev. D **100**, 083517 (2019).
[56] S. Pan, W. Yang, E. Di Valentino, E. N. Saridakis, and S. Chakraborty, Interacting scenarios with dynamical dark energy: Observational constraints and alleviation of the H_0 tension, Phys. Rev. D **100**, 103520 (2019).
[57] F. K. Anagnostopoulos, S. Basilakos, and E. N. Saridakis, Observational constraints on Barrow holographic dark energy, Eur. Phys. J. C **80**, 826 (2020).
[58] J. Alfaro, M. San Martín, and C. Rubio, Observational constraints in delta gravity: CMB and supernovas, Astrophys. J. **910**, 43 (2021).
[59] F. Felegary, I. A. Akhlaghi, and H. Haghi, Evolution of matter perturbations and observational constraints on tachyon scalar field model, Phys. Dark Universe **30**, 100739 (2020).
[60] E. Di Valentino, A (brave) combined analysis of the H_0 late time direct measurements and the impact on the Dark Energy sector, Mon. Not. R. Astron. Soc. **502**, 2065 (2021).
[61] A. Paliathanasis, S. Basilakos, E. N. Saridakis, S. Capozziello, K. Atazadeh, F. Darabi, and M. Tsamparlis, New Schwarzschild-like solutions in $f(T)$ gravity through Noether symmetries, Phys. Rev. D **89**, 104042 (2014).
[62] A. Paliathanasis, $f(R)$-gravity from killing tensors, Classical Quantum Gravity **33**, 075012 (2016).
[63] N. Dimakis, A. Karagiorgos, A. Zampeli, A. Paliathanasis, T. Christodoulakis, and P. A. Terzis, General analytic solutions of scalar field cosmology with arbitrary potential, Phys. Rev. D **93**, 123518 (2016).
[64] H. Yu, B. Ratra, and F. Y. Wang, Hubble parameter and baryon acoustic oscillation measurement constraints on the Hubble constant, the deviation from the spatially flat ΛCDM model, the deceleration/acceleration transition redshift, and spatial curvature, Astrophys. J. **856**, 3 (2018).
[65] M. Moresco, R. Jimenez, L. Verde, L. Pozzetti, A. Cimatti, and A. Citro, Setting the stage for cosmic chronometers. I. Assessing the impact of young stellar populations on Hubble parameter measurements, Astrophys. J. **868**, 84 (2018).
[66] D. M. Scolnic, D. O. Jones, A. Rest, Y. C. Pan, R. Chornock, R. J. Foley, M. E. Huber, R. Kessler, G. Narayan, A. G. Riess *et al.*, The complete light-curve sample of spectroscopically confirmed SNe Ia from Pan-STARRS1 and cosmological constraints from the combined pantheon sample, Astrophys. J. **859**, 101 (2018).
[67] R. Kessler and D. Scolnic, Photometrically identified samples, Astrophys. J. **836**, 56 (2017).
[68] D. J. Eisenstein and W. Hu, Baryonic features in the matter transfer function, Astrophys. J. **496**, 605 (1998).
[69] S. Alam *et al.* (eBOSS Collaboration), The Completed SDSS-IV extended baryon oscillation spectroscopic survey: Cosmological implications from two decades of spectroscopic surveys at the apache point observatory, Phys. Rev. D **103**, 104013 (2021)..
[70] J. Ryan, Y. Chen, and B. Ratra, Baryon acoustic oscillation, Hubble parameter, and angular size measurement constraints on the Hubble constant, dark energy dynamics, and spatial curvature, Mon. Not. R. Astron. Soc. **488**, 3844 (2019).
[71] D. F. Torres, H. Vucetich, and A. Plastino, Early Universe Test of Nonextensive Statistics, Phys. Rev. Lett. **79**, 1588 (1997); , Erratum, Phys. Rev. Lett. **80**, 3889 (1998).
[72] G. Lambiase, Lorentz invariance breakdown and constraints from big-bang nucleosynthesis, Phys. Rev. D **72**, 087702 (2005).
[73] J. D. Barrow, S. Basilakos, and E. N. Saridakis, Big bang nucleosynthesis constraints on Barrow entropy, Phys. Lett. B **815**, 136134 (2021).
[74] N. Aghanim *et al.* (Planck Collaboration), Planck 2018 results. VI. Cosmological parameters, Astron. Astrophys. **641**, A6 (2020).
[75] J. Goodman and J. Weare, Ensemble samplers with affine invariance, Commun. Appl. Math. Comput. Sci. **5**, 65 (2010).
[76] D. Foreman-Mackey, D. W. Hogg, D. Lang, and J. Goodman, emcee: The MCMC Hammer, Publ. Astron. Soc. Pac. **125**, 306 (2013).
[77] H. Akaike, A new look at the statistical model identification, IEEE Trans. Autom. Control **19**, 716 (1974).
[78] G. Schwarz, Estimating the dimension of a model, Ann. Stat. **6**, 461 (1978).
[79] D. J. Spiegelhalter, N. G. Best, B. P. Carlin, and A. Van Der Linde, Bayesian measures of model complexity and fit, J. R. Stat. Soc. **64**, 583 (2002).
[80] R. Andrae, T. Schulze-Hartung, and P. Melchior, Dos and don'ts of reduced chi-squared, arXiv:1012.3754.
[81] K. Anderson, *Model Selection and Multimodel Inference: A Practical Information-Theoretic Approach*, 2nd ed. (Springer, New York, 2002).
[82] K. P. Burnham and D. R. Anderson, Multimodel inference: Understanding AIC and BIC in model selection, Sociol. Methods Res. **33**, 261 (2004).
[83] A. R. Liddle, Information criteria for astrophysical model selection, Mon. Not. R. Astron. Soc. **377**, L74 (2007).
[84] R. E. Kass and A. E. Raftery, Bayes factors, J. Am. Stat. Assoc. **90**, 773 (1995).

[85] S. Cao, J. Ryan, and B. Ratra, Using Pantheon and DES supernova, baryon acoustic oscillation, and Hubble parameter data to constrain the Hubble constant, dark energy dynamics, and spatial curvature, Mon. Not. R. Astron. Soc **504**, 300.

[86] A. G. Riess *et al.*, A 2.4% determination of the local value of the Hubble constant, Astrophys. J. **826**, 56 (2016).

[87] S. Birrer, A. J. Shajib, A. Galan, M. Millon, T. Treu, A. Agnello, M. Auger, G. C. F. Chen, L. Christensen, T. Collett *et al.*, TDCOSMO—IV. Hierarchical time-delay cosmography—joint inference of the Hubble constant and galaxy density profiles, Astron. Astrophys. **643**, A165 (2020).

[88] W. L. Freedman, B. F. Madore, T. Hoyt, I. S. Jang, R. Beaton, M. G. Lee, A. Monson, J. Neeley, and J. Rich, Calibration of the tip of the red giant branch (TRGB), arXiv:2002.01550.

[89] G. Chen and B. Ratra, Median statistics and the Hubble constant, Publ. Astron. Soc. Pac. **123**, 1127 (2011).

[90] M. Rigault, G. Aldering, M. Kowalski, Y. Copin, P. Antilogus, C. Aragon, S. Bailey, C. Baltay, D. Baugh, S. Bongard *et al.*, Confirmation of a star formation bias in type Ia supernova distances and its effect on measurement of the Hubble constant, Astrophys. J. **802**, 20 (2015).

[91] Y. Chen, S. Kumar, and B. Ratra, Determining the Hubble constant from Hubble parameter measurements, Astrophys. J. **835**, 86 (2017).

[92] B. R. Zhang, M. J. Childress, T. M. Davis, N. V. Karpenka, C. Lidman, B. P. Schmidt, and M. Smith, A blinded determination of H_0 from low-redshift Type Ia supernovae, calibrated by Cepheid variables, Mon. Not. R. Astron. Soc. **471**, 2254 (2017).

[93] S. Dhawan, S. W. Jha, and B. Leibundgut, Measuring the Hubble constant with Type Ia supernovae as near-infrared standard candles, Astron. Astrophys. **609**, A72 (2018).

[94] D. Fernández Arenas, E. Terlevich, R. Terlevich, J. Melnick, R. Chávez, F. Bresolin, E. Telles, M. Plionis, and S. Basilakos, An independent determination of the local Hubble constant, Mon. Not. R. Astron. Soc. **474**, 1250 (2018).

[95] K. Blum, E. Castorina, and M. Simonović, Could quasar lensing time delays hint to a core component in halos, instead of H_0 tension?, Astrophys. J. Lett. **892**, L27 (2020).

[96] O. Farooq, F. R. Madiyar, S. Crandall, and B. Ratra, Hubble parameter measurement constraints on the redshift of the deceleration–acceleration transition, dynamical dark energy, and space curvature, Astrophys. J. **835**, 26 (2017).

[97] M. Rezaei, S. Pour-Ojaghi, and M. Malekjani, A cosmography approach to dark energy cosmologies: New constraints using the Hubble Diagrams of supernovae, quasars, and gamma-ray bursts, Astrophys. J. **900**, 70 (2020).

[98] B. S. Haridasu, V. V. Lukovi ć, M. Moresco, and N. Vittorio, An improved model-independent assessment of the late-time cosmic expansion, J. Cosmol. Astropart. Phys. 10 (2018) 015.